A Feedback Control System for Suppressing Crane Oscillations with On-Off Motors

Keith A. Hekman and William E. Singhose

Abstract: Crane payloads frequently swing with large amplitude motion that degrades safety and throughput. Open-loop methods have addressed this problem, but are not effective for disturbances. Closed-loop methods have also been used, but generally require the speed of the driving motors to be precisely controlled. This paper develops a feedback control method for controlling motors to cancel the measured payload oscillations by intelligently timing the ensuing on and off motor commands. The effectiveness of the oscillation suppression scheme is experimentally verified on an industrial bridge crane.

Keywords: Crane control, non-linear feedback, on-off control, vibration suppression.

1. INTRODUCTION

Cranes are frequently used to transport heavy objects in a cluttered workspace. One inherent problem with cranes is that the payload can swing freely. These oscillations pose safety hazards and can damage the payload or other objects in the workplace. Traditionally, an experienced crane operator is required to keep the oscillations under control. More recently, various control approaches have been applied to augment the operator's skill. These approaches fall into open and closed-loop categories.

One open-loop approach is input shaping, which has proven effective on cranes for reducing sway during and after the move [1-3], including during hosting [4]. Shapers can be designed with robustness to modeling inaccuracies [5] (i.e., cable length changing the oscillation frequency). Another open-loop approach is optimal control, which calculates a motion trajectory off line based on the mathematical model of the system [6,7]. However, if the model is inaccurate, the performance will suffer. This is also the case with input shaping, but to a lesser degree. In addition, optimal control has not been used with current crane operator interfaces, as the path is not generally known beforehand.

System model uncertainties and external disturbances provide the motivation for feedback control. Controllers have used the position and velocity of the trolley and the cable swing angle [8-11] or the spreader inclination [12] to reduce payload oscillations. Wave absorption control adjusts the trolley velocity to absorb any waves that are being returned by the payload, thereby canceling the oscillation [13]. Feeding a delayed angle measurement back to the desired position has also been shown effective in reducing payload oscillations [14].

Sorenson *et al.* [15,16] developed a control system that combined input shaping and PD feedback control. The feedback control used measurements from an overhead camera and compared the measured crane response to the modeled shaped response.

Although not directly crane control, Park and Chang [17] proposed another method to reduce the effect of a disturbance on a vibrating system. They developed a "commandless" input shaping method for a telescopic handler. To compensate for the vibrations from unloading the handler, they introduce a pulse that induces vibration equal in magnitude but opposite in phase of the vibration caused by unloading. They show the method's potential by using it to reduce vibration by about 75%. However, issues of properly timing the pulse and ease of calibration appear to be challenging.

All of the feedback methods described above require the velocity or acceleration of the crane trolley to be precisely controlled. The research presented here is based on using measurement of payload swing to

Manuscript received August 1, 2006; revised March 11, 2007; accepted March 27, 2007. Recommended by Editorial Board member Jang Myung Lee under the direction of Editor Jae Weon Choi. Siemens Energy and Automation supported this work. They provided all of the equipment necessary in implementing the crane control. Furthermore, they provided financial support for graduate students to install and program the controller. Dr. Hekman was supported by the American University in Cairo, Egypt, where he was part of the faculty during this research.

Keith A. Hekman is with the Engineering Department, Calvin College, Grand Rapids, MI 49546 USA (e-mail: hekman@calvin.edu).

William E. Singhose is with the George W. Woodruff School of Mechanical Engineering, The Georgia Institute of Technology, Atlanta GA 30332 USA (e-mail: William.Singhose@me.gatech.edu).

generate commands for on-off motors to cancel the payload swing, making it applicable to a broad range of cranes. This method could be added to existing cranes without modifying its motor drive system, but only passing the operators commands (go forward, go backwards) through the controller.

2. VECTOR BASED INPUT SHAPER CALCULATION

Although the controller developed here is closed-loop, the mathematics behind the controller is similar to that of vector-based input-shaping calculations, an open-loop method. The basic concept behind input shaping is that a later motion can cancel oscillations excited by an earlier motion. Fig. 1 shows the response of a lightly damped system to two impulses. The first impulse excites a decaying oscillation. A second impulse, if it is properly sized and delayed, will excite an oscillation equal to the first, but opposite in magnitude. When this is superimposed over the first response, the result is no net oscillation after the second impulse, as seen by the total response line.

In reality, systems are not moved with impulses. To create a practical command, the impulse sequence is convolved with the desired command. By this process the original command is input-shaped into a command that will also not produce any residual vibrations after the shaped command is completed. For example, Fig. 2 shows that when a step command is convolved with two impulses it produces a staircase command. After time Δ, the system will have no residual oscillations.

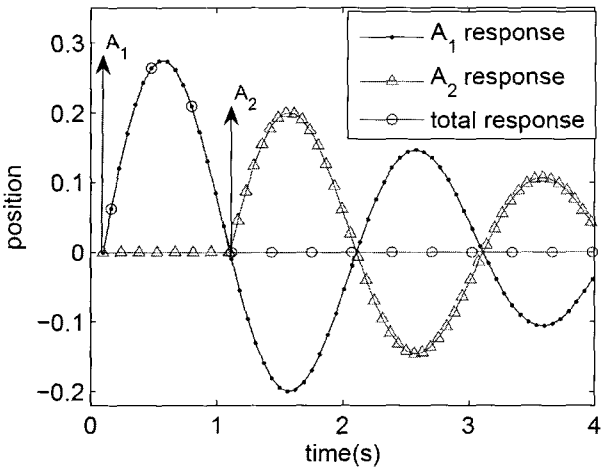

Fig. 1. A second impulse can cancel induced vibration.

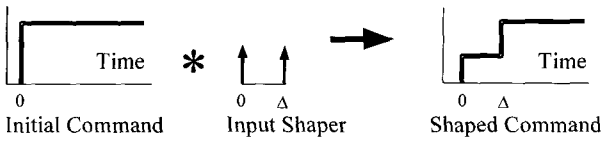

Fig. 2. Creating a stair step command by convolution.

Den Hartog [18] and Booker [19] provide a framework for analyzing oscillations with vectors. Singhose *et al.* [20] provide insight into how vibration cancellation can be achieved in a vector-based analysis of input shapers. An impulse of magnitude A_1 applied to an undamped second-order system of unit mass will induce a response of

$$x(t) = A_1 \sin \omega t. \tag{1}$$

This response has a magnitude A_1 and phase angle of zero. Similarly, if a second impulse of magnitude A_2 is applied at time t_2, then it will result in an output of.

$$x(t) = A_2 \sin \omega(t - t_2) = A_2 \sin(\omega t - \omega t_2), \quad t > t_2. \tag{2}$$

This response has a magnitude A_2 and phase angle $\theta_2 = \omega t_2$. The magnitudes and angles of the responses can be transformed into vector notation as seen in Fig. 3. Summing these vectors gives a representation of the total vibration response, as shown in Fig. 4. The corresponding time response to these impulses is shown in Fig. 5. After the second impulse, the total

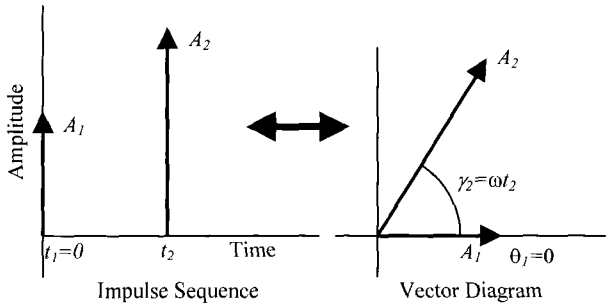

Fig. 3. Impulse sequence and corresponding vector diagram.

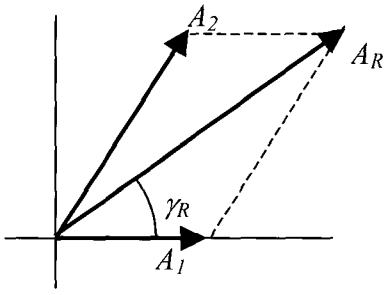

Fig. 4. Summing two vectors to get the total response.

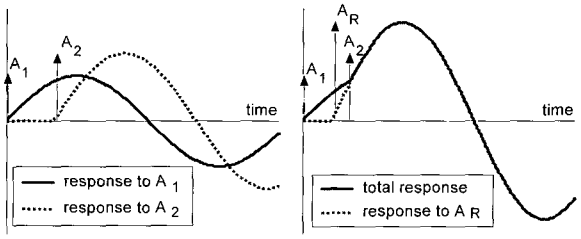

Fig. 5. Time response of impulses (adapted from [20]).

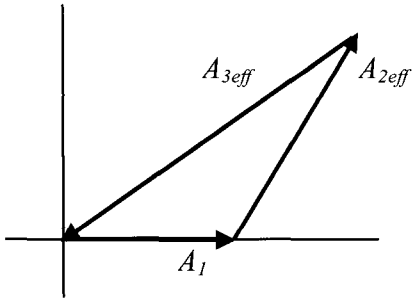

Fig. 6. Summing three vectors to get zero vibration.

response matches the amplitude and phase of the resultant vector A_R, shown in Fig. 4.

If the system has damping, then this method needs to be modified. First, the vector angle γ_i changes to

$$\gamma_i = \sqrt{1-\zeta^2}\,\omega t_i. \tag{3}$$

Second, damping causes the oscillation amplitude to decay over time. To account for the decay, the vector amplitudes must be scaled using the times at which they occur. To calculate the combined effect from several impulses, they can be transferred back to t=0. The effective amplitude of the vector at t=0 is

$$A_{eff} = Ae^{\zeta\gamma_i/\sqrt{1-\zeta^2}} \tag{4}$$

with time in γ_i defined by (3).

An input shaper can be designed such that the sum of all the effective impulses results in zero vibration, as demonstrated with three vectors in Fig. 6. To accomplish the cancellation, the A_{3eff} is chosen to be the negative of the vector A_R from Fig. 4. To get the magnitude of this canceling impulse, it must be converted to the time it will occur using (3) and

$$A_3 = A_{3eff}e^{-\zeta\gamma_i/\sqrt{1-\zeta^2}}. \tag{5}$$

3. PAYLOAD OSCILLATION CANCELLATION

The goal of this research is not to create commands that result in zero residual oscillation for point-to-point motion. Rather, the measured payload swing is used to generate on-off commands for motors that will cancel payload swing once it occurs. When creating such commands, the magnitude of the motor torque cannot be arbitrarily chosen, as the motor can only be turned on and off. However, turning the motor on or off will cause payload oscillations, which can be represented as vectors. Unlike a pure impulse, these vectors will not have zero phase angles, as the motor does not instantly stop or accelerate to full speed. Therefore, by the time the command is completed, the payload will have some angular displacement (θ) and some angular velocity ($\dot{\theta}$), giving a vector representation similar to Fig. 7. The velocity term is scaled by the oscillation frequency, since an undamped system with peak displacement θ has a peak velocity amplitude of $\omega\theta$.

The vector for turning the motor off should have a similar magnitude, but in the opposite direction, assuming that the acceleration and deceleration dynamics are similar. If not, deceleration can be represented by its own unique amplitude and phase.

The controller developed here will use two motor command switches (on-off) to eliminate payload oscillation. The appropriate times of these switches need to be calculated in real time. The controller continually monitors the current level of payload swing angle and its derivative to determine the proper time to make the corrective action.

To make this calculation, a vector triangle is used, as seen in Fig. 8, which shows the two possible timings to cancel vibrations. The first side of the triangles in both Fig. 8(a) and 8(b) is the current oscillation level (A_{vib}). The oscillation amplitudes of "on" and "off" motor commands form the other two sides of the triangles. If the three sides can form a closed triangle, then the oscillation can be forced back

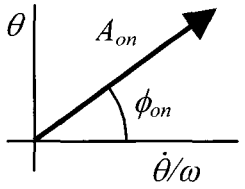

Fig. 7. Vector representation for turning the motor on.

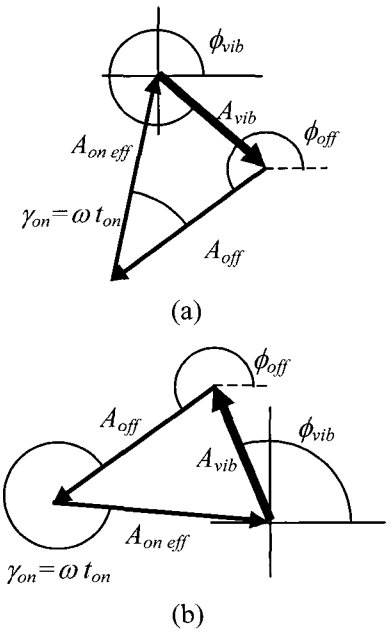

Fig. 8. Vector diagram for calculating time to turn motor off.

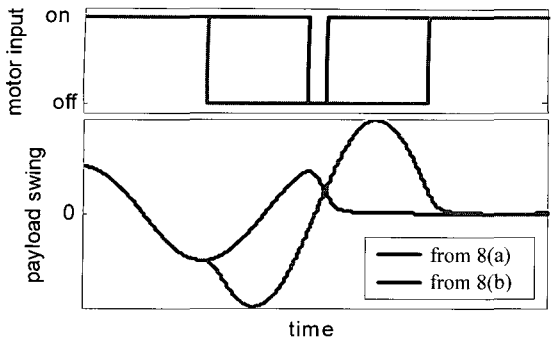

Fig. 9. Time responses from commands represented in Fig. 8.

to zero (the origin of the vector diagram) with an "off" motor command at that instant. Assuming that the human operator wants the crane to be moving and has the "on" button pressed, then the command sequence issued by the controller would be "off", wait, then "on" again.

Certain components of the triangles are known: the magnitude of the current oscillation and the effect of turning the crane on (A_{on}) and off (A_{off}). The vector for A_{off} is fixed at the instant the motor is turned off, while the direction of the vector for A_{on} can be altered by changing the time until the crane is turned back "on" again (t_{on}). Waiting to initiate the control action changes the phase angle of the current oscillation (ϕ_{vib}). As stated before, there are two possible solutions to form this triangle, as shown in Fig. 8. The time responses of these two solutions are shown in Fig. 9. The solution in Fig. 8(a) is preferable because it has a smaller angle $\gamma_{on}=\omega t$, so the wait time until the motor is turned back on to cancel the oscillations is shorter. Also, the maximum swing angle of the response is less, assuming that the existing vibration is lower than the oscillation induced by a change in state of the trolley. For these reasons, the timing in Fig. 8(a) is always used.

To find the phase angle of the current oscillations (ϕ_{vib}) for the "off" motor command the intermediate angles γ_{on} and δ shown in Fig. 10 are used. From the law of cosines,

$$A_{oneff}^2 = A_{off}^2 + A_{vib}^2 - 2A_{off}A_{vib}\cos\delta, \quad (6)$$

$$A_{vib}^2 = A_{off}^2 + A_{oneff}^2 - 2A_{off}A_{oneff}\cos\gamma_{on}. \quad (7)$$

Solving (7) for γ_{on} yields

$$\gamma_{on} = \cos^{-1}\left(\frac{A_{off}^2 + A_{oneff}^2 - A_{vib}^2}{2A_{off}A_{oneff}}\right) \quad (8)$$

If there is no damping, then the solution can be solved algebraically since $A_{on\,eff}=A_{on}$. Note that most cranes have near zero damping, but if the damping is significant, then the same equation can be used to

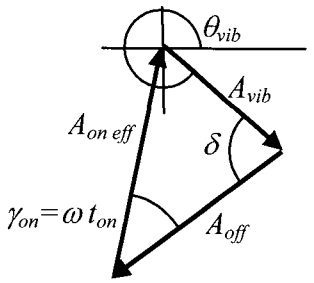

Fig. 10. Angles used to calculate command initiation time.

solve for γ_{on}; however, since it is nonlinear, it must be solved iteratively, using

$$A_{oneff} = A_{on}e^{\zeta\gamma_{on}/\sqrt{1-\zeta^2}}. \quad (9)$$

(8) is initially calculated using ζ=0. After γ_{on} is found, δ from Fig. 9 can be calculated using

$$\delta = \cos^{-1}\left(\frac{A_{off}^2 + A_{vib}^2 - A_{oneff}^2}{2A_{off}A_{vib}}\right). \quad (10)$$

Once δ is known, the phase angle of the current oscillation (γ_{vib}) for the "off" command can be calculated using

$$\phi_{vib} = \phi_{off} - \delta + \pi. \quad (11)$$

After the trolley has stopped, the payload swing should have the same magnitude as that induced when the motor is turned back on. The controller then waits until the angle of the payload oscillation (ϕ_{vib}) is opposite in direction to the phase angle of the oscillation induced by turning the motor on (ϕ_{on}.) At this point, the controller turns the motor back on and the trolley starts moving again. If the calibration is perfect, the payload oscillations will be completely eliminated. If the calibration is imperfect, (and it always is), then some oscillations will remain, but a large portion will be canceled out by the control action.

If the operator desires the crane to be stopped, then no control buttons are pressed. Any existing payload oscillations can be canceled by moving the overhead support either forward or backward. This situation results in two different phase angles of payload swing that can be used by the controller, as shown in Fig. 11, with the subscripts r and f denoting reverse and forward. In the reverse direction, the diagram is the same as Fig. 8(a), except the "on" and the "off" are exchanged. Based on this vector triangle,

$$\gamma_{off} = \cos^{-1}\left(\frac{A_{on}^2 + A_{off\,eff}^2 - A_{vib}^2}{2A_{on}A_{off\,eff}}\right), \quad (12)$$

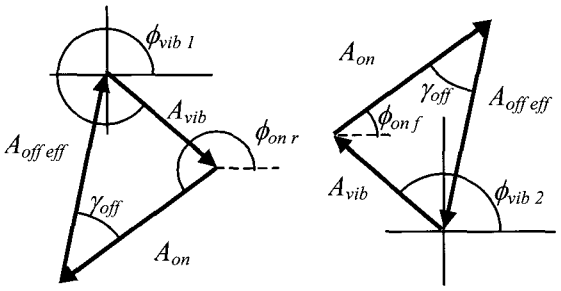

(reverse) (forward)

Fig. 11. Vector diagram for when to turn on motor.

$$\delta = \cos^{-1}\left(\frac{A_{on}^2 + A_{vib}^2 - A_{off\,eff}^2}{2A_{on}A_{vib}}\right), \tag{13}$$

$$\phi_{vib1} = \phi_{on} - \delta + \pi \tag{14}$$

with δ still describing the interior angle between A_{vib} and A_{on}.

For the forward direction, the vector triangle has the same geometry only it is rotated by π radians. Therefore,

$$\phi_{vib2} = \phi_{on\,f} - \delta + \pi. \tag{15}$$

The controller compares the existing vibration phase angle to (14) and (15) and takes corrective action at whichever phase angle occurs first. Once the crane is moving, then the controller waits until the oscillation phase angle is opposite to that of the appropriate "off" command, ϕ_{off}, at which point the trolley motor is stopped.

The maximum oscillation magnitude that can be canceled using an on-off command is approximately twice the oscillation induced by an "on" command. If the current oscillation magnitude is larger than this value, then the controller calculations are based on the maximum cancellation level. Above this limit, δ is set to zero in the calculations for ϕ_{on} and ϕ_{off}. As a precaution, this maximum level can be reduced to limit the distance moved by the trolley in canceling the oscillations, thus limiting the angle γ_{on} and t_{on}.

Differences between the physical system response and the response during calibration will result in non-zero residual oscillations after a single control action. Very large payloads that slightly decrease the crane response time could cause these differences. Extreme calibration error could also lead to an undesirable limit cycle. Three types of calibration errors that can occur are in the magnitude of A_{on} and A_{off}, in the phase angle of A_{on} and A_{off}, and a difference in the oscillation frequency. For the control calculation for when to turn off the motor, vector diagrams of residual oscillation for calibration differences in both magnitude and phase are shown in Fig. 12. The dotted arrows represent the controller calibration, and the solid

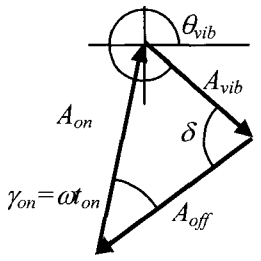

(a) Control calculation.

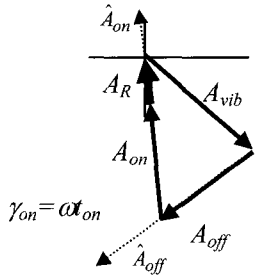

(b) Residual oscillation with error in vector magnitudes.

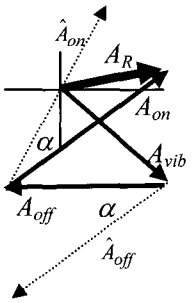

(c) Residual oscillation with error in vector angles.

Fig. 12. Residual oscillations from calibration errors in A_{on} and A_{off}.

arrows represent the actual induced oscillation by the motor. The residual oscillation vector is denoted by A_R. The original vector triangle is shown for reference. Similar triangles can be constructed when to turn on the motor when the desired motion is "off".

The difference in vector magnitude is the least problematic. A typical control action would be for the user to press the go button, and then the controller would perform an off-on sequence to remove the resulting oscillations. To gage the effectiveness of the control action, Fig. 13 shows the oscillation reduction ratio for one control action vs. the ratio of the modeled amplitude to the actual amplitude. For a ratio of 1, there is no residual vibration. For regions around 1, there is a significant reduction in the oscillations after a single control sequence. In all cases, the oscillations would approach zero asymptotically with repeated control actions. However, this is not acceptable, as the crane motion of several off-on sequences would result in significant loss of efficiency. Therefore, an oscillation magnitude set point should be used to limit the operation of the controller to moderate and large oscillations.

Differences in the phase calibration of A_{on} and A_{off} cause the most difficulty for the controller. A vector diagram of the effects was shown in Fig. 12. For each of the response vectors, the calibration error shifts the actual response by an angle α from the controller calculation. For the off-on control response, the off

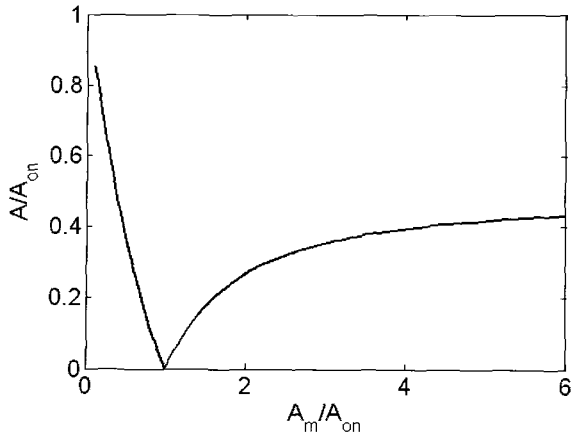

Fig. 13. Oscillation reduction ratio vs. ratio of modeled and actual induced vibrations for one controller action.

command is initiated when the controller calculates the calibrated vector triangle. The phase shift causes the ensuing motion to have a different phase, and amplitude. The controller then switches back on the trolley when it calculates the current oscillation vector is opposite to A_{on}. This results in a nonzero residual oscillation, since the actual response is shifted by an angle α. The oscillation magnitude ratio after one on-off control command is plotted to verify the robustness of the control scheme vs. calibration difference in the phase angle of A_{on} and A_{off}. Unlike the magnitude error, the steady state oscillation magnitude will not be zero, but rather a limit cycle will occur if no control action threshold is utilized. At the limit cycle, the oscillation magnitude is not reduced by the control action, only the phase is changed. The magnitude of the limit cycle is plotted in Fig. 14. It is critical that the controller action threshold be above this limit, or the crane will continually start and stop. The plot shows that for angles of -40° and 60° the control action will have a limit cycle equal to that of initiating the motion of the trolley. Between these limits, there is a reasonable reduction in payload swing.

Any error in the estimate of the oscillation frequency ω creates an error in the estimation of the current oscillation magnitude. The vector diagram for this case is shown in Fig. 15. The velocity component of the vector would be scaled inappropriately, which gives the horizontal shift between actual oscillation level A_{vib} and the calculated level $\hat{A}_{vib}$. If the payload is swinging at a constant amplitude, it would appear as if the magnitude is rising and falling. When the second control action takes place, the phase would also be incorrect, causing an improper timing of turning back on the motor. This shift β can be calculated using

$$\beta = \tan^{-1}\left(\frac{\tan\phi_{on}}{\omega/\omega_m}\right) - \phi_{on}. \tag{16}$$

The resulting oscillation level reduction can be plotted vs. the ratio between the actual and modeled frequency of oscillation as seen in Fig. 16. Since β is dependent on ϕ_{on}, the calculation is done using the ϕ_{on} calculated experimentally for the crane described in Section 4. As long as the model frequency is larger than the actual frequency, there is no danger of going

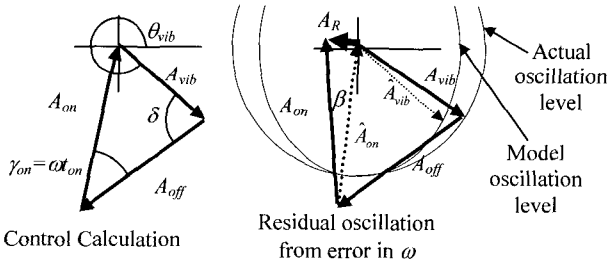

Fig. 15. Residual oscillations from incorrect estimation of oscillation frequency.

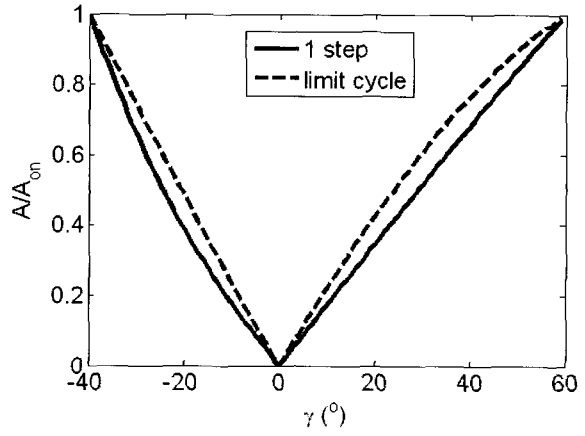

Fig. 14. Oscillation reduction ratio vs. calibration phase error in ϕ_{on}.

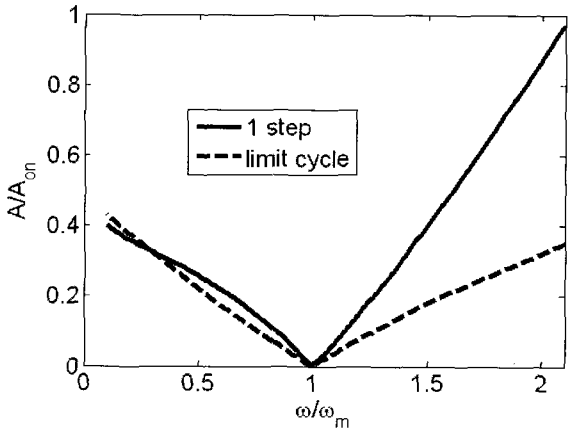

Fig 16. Oscillation reduction ratio vs. ratio of actual (ω) and modeled (ω_m) oscillation frequency.

unstable. The controller also provides a reduction in oscillation until the model frequency is half the actual frequency. Good oscillation reduction is achieved with a frequency error of plus or minus 50% of the model frequency.

The addition of a large payload mass may cause the crane to respond differently than the model estimates. The additional mass would cause the system to accelerate more slowly, leading to a smaller amplitude of oscillation A_{on}. Also, the slower acceleration will lead to a positive γ, which is the direction of greater stability. Finally, if the additional mass was significantly lower than the hook, it would reduce the oscillation frequency ω of the physical system. This too is in the direction of greater stability. Overall, the control can be expected to work well over a broad range of payload sizes.

4. CONTROLLER IMPLEMENTATION

The oscillation cancellation techniques from Section 3 were implemented on a large bridge crane at the Georgia Institute of Technology. Fig. 17 shows a picture of the crane. As seen in the image, the crane has a camera mounted on the trolley to measure the payload swing in the horizontal plane. In addition to the swing angle, the camera can measure the length of cable height of the payload. Hekman *et al.* [15] provide a detailed development of the use of a camera to measure the swing angle of the hook.

The crane is 10 meters wide by 43 meters long and 6 meters high, with a maximum load of 10 tons. There is a Siemens asynchronous induction motor driving the trolley and two driving the bridge. The motors are powered by Siemens Simovert Master Drive converters. A Siemens Simatic S7-300 PLC processes the input from the crane pendant and the controller that was implemented on a PC and gives the reference velocity to the vector control drive. An Ethernet network enabled communication between the PC, PLC and vision system.

4.1. System calibration

The controller calculations (8)-(15) require the magnitude and phase angle of the oscillations caused by turning the motor "on" and "off". These can be calculated by plotting the crane input and the payload response on the same graph, as in Fig. 18. The top of Fig. 18 shows the motor being turned off at about 5.5 seconds while the crane is moving forward. The trolley takes about one second to come to rest after the command is issued. The bottom of the figure shows the payload swing angle θ and the oscillation level m given by

$$m = \sqrt{\theta^2 + \left(\dot{\theta}/\omega\right)^2}, \tag{17}$$

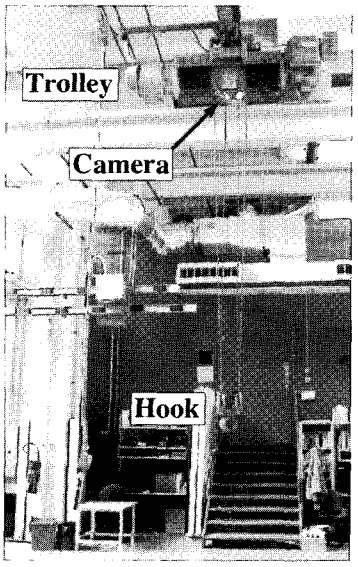

Fig. 17. Bridge crane.

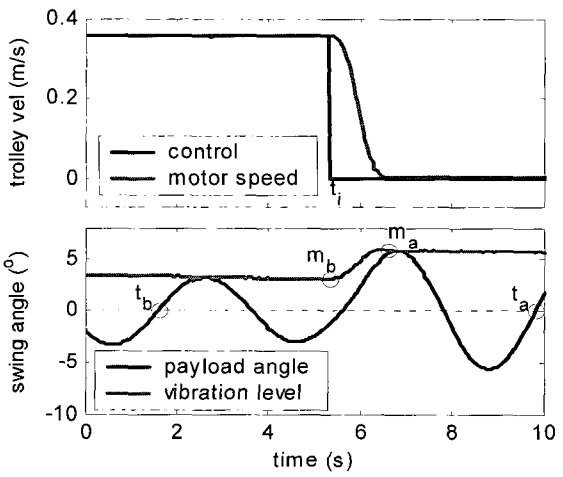

Fig. 18. Measured bridge crane response to an "off" command.

where ω is the frequency of the payload oscillation.

The times of the rising zero crossing of the swing angle before (t_b) and after (t_a) the input change (t_i) were recorded. The zero crossing at about 6 seconds was not used, because the motor speed was in transition. The phase angles of the oscillation before (ϕ_b) and after (ϕ_a) the input change can be calculated using

$$\phi_b = \frac{2\pi\left(t_b + T_p - t_i\right)}{T_p}, \quad \phi_a = \frac{2\pi\left(t_a - T_p - t_i\right)}{T_p}, \tag{18}$$

where T_p is the time of one oscillation period. The vector representing the input transition can be calculated using a complex number representation with the real portion being the velocity component $\dot{\theta}/\omega$ and the imaginary part the position component θ. The input transition vector is given by

$$A_{off}e^{i\phi_{off}} = m_a e^{-i\phi_a} - m_b e^{-i\phi_b}, \quad (19)$$

where m_b and m_a are the amplitudes of the oscillation before and after the transition. A similar procedure can be used to determine the "off" vector in the reverse direction and the "on" vector in both the forward and reverse directions.

Graphically, the induced oscillation vectors can be plotted for starting and stopping, for both forward and reverse directions, as seen in Fig. 19. For a 4 meter cable length, on average the oscillation had an amplitude of 0.052 radians at an angle of ϕ=1.11(+π) radians (63.6 (+180)°).

To examine the variation in the response of the crane and payload under for different operating conditions, the motion of the crane and payload was recorded during "on" and "off" commands. The tests were performed at two different cable lengths (3.5m and 5.5m) and additional payload masses between zero and 227 kg (500 lbs) above the nominal hook weight of 50 kg (110 lbs). These represent typical operating conditions of a crane an industrial setting. The vectors A_{on} and A_{off} were calculated at each combination, as well as the oscillation frequency.

Fig. 20 shows the variation in the vector magnitude. The data does not show any strong trends for the magnitude variation over the range of mass tested. The maximum ratio between the A_m/A_{on} is1.37 which has a residual oscillation level of less than 10% of a single state transition based on Fig. 13.

Fig. 21 shows the variation in the vector phase angle for the different test conditions. There is about a 20° shift in phase for a single height and a 43° over both heights. For the +-10° shift, from Fig. 14, the residual oscillation level of about 15% is quite good. At +-22°, the residual oscillation level of about 50% could be acceptable, though not preferable. Therefore, the controller effectiveness is improved by incorporating the payload height into its calculations.

Fig. 22 shows the variation in the oscillation frequency caused by changes in payload mass and cable length. At a specific cable length, the ratio between the minimum and maximum frequency is about 0.9, which according to Fig. 16, will produce negligible residual oscillations. If the cable length is not taken into account in the controller calculations, then the ratio is 0.73, which has a residual oscillation level of about 15% of a single state change A_{on}.

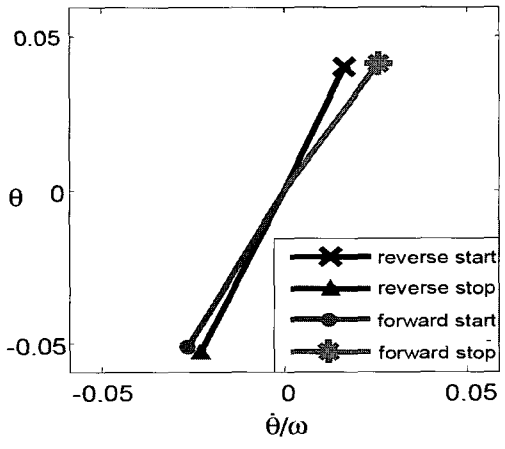

Fig. 19. Oscillation vectors for different commands.

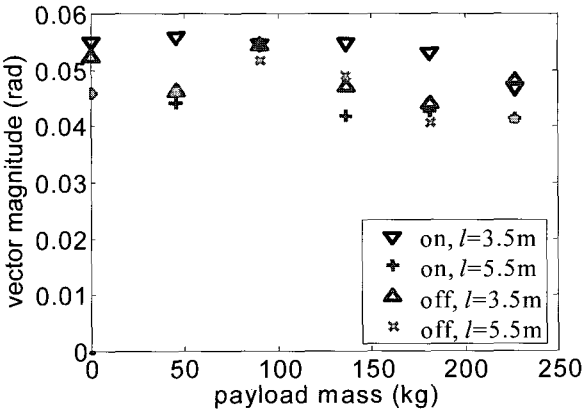

Fig 20. Vector magnitude variation with payload mass and cable length l.

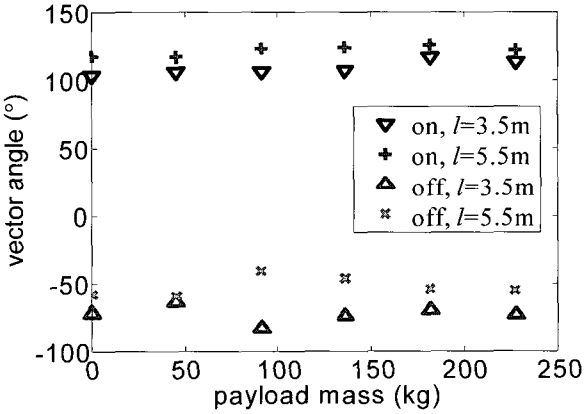

Fig 21. Vector phase angle variation with payload mass and cable length l.

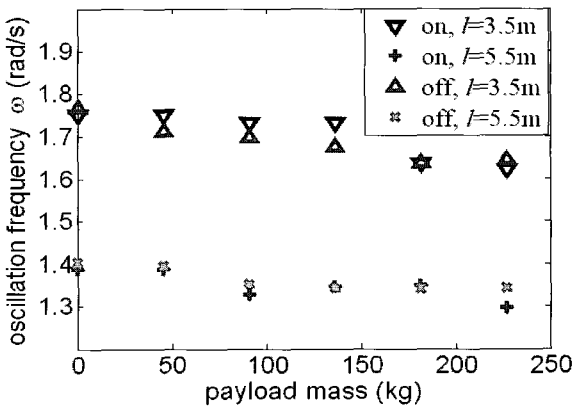

Fig. 22. Vector oscillation frequency variation with payload mass and cable length l.

4.2. Controller response for user motion

Fig. 23 shows a typical crane motion and the corresponding payload swing. The "go" button is pressed at about 2 seconds and is released at about 8 seconds, as indicated by the commanded velocity line. The initial motion of the trolley caused the payload to swing with a magnitude of 3°. When the trolley stopped, more oscillations were excited, increasing the total magnitude of payload swing to about 4°. At a cable length of 5.5m the 4° of swing correlates to over a half meter of peak-to-peak motion. Further actions by the user could either excite more oscillations or cancel out the oscillations, depending on their timing. With an inexperienced operator, these oscillations can quickly become quite large.

Fig. 24 shows the response of the controlled crane to a user request to move backward. In the top plot in Fig. 24, the user input is shown using a line with circles. The resulting trolley speed is shown with a dashed line. As shown in the middle plot of Fig. 24, the crane motion excites oscillations in the payload. However, the controller makes corrective actions at about 6 seconds and at about 14 seconds. Both actions are effective at reducing the payload swing, both during the requested motion and after the crane has been stopped. The bottom part of Fig. 24 shows the phase angle of the oscillations given by

$$\phi = \tan^{-1}\left(\frac{\theta}{\dot{\theta}/\omega}\right). \tag{20}$$

The bottom plot also shows the switch angle calculated from (11)-(15). At the initial crossing (near 2 seconds), the oscillation amplitude is not large enough (1.7°) to trigger a control action. It is one period later (at about 6 seconds) that the oscillation-canceling control action takes place. At this point, the controller briefly turns off the crane motor, as seen in the top plot of Fig. 24. At this point the switch angle jumps to ϕ_{on}. At 7 seconds, this angle occurs, and the crane motor is turned back on. When the trolley

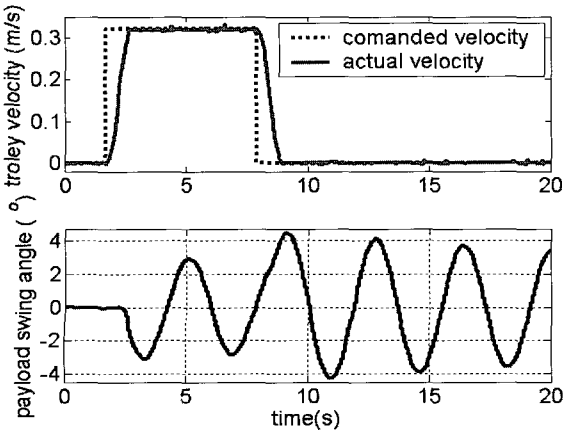

Fig. 23. Typical uncontrolled response.

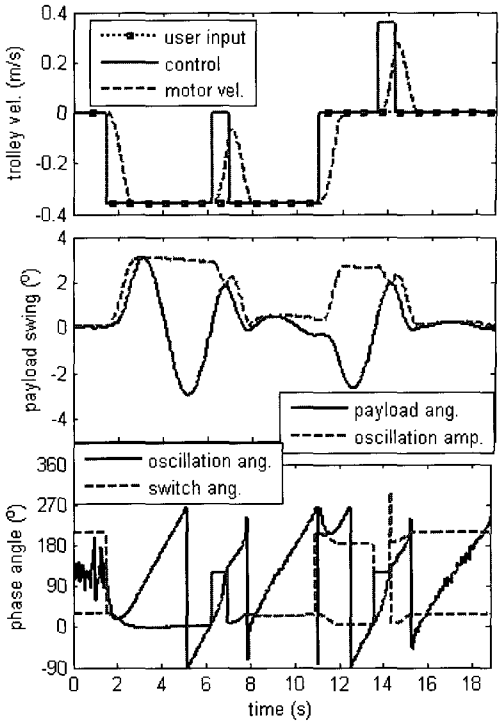

Fig. 24. Response to an operator commanding reverse motion.

reaches full speed (at about 8 seconds), the oscillation level is quite small (about a half degree) as shown in the middle plot of Fig. 24.

The operator stops pressing the reverse button at about 11 seconds, as shown by the solid line in the top plot of Fig. 24. When the trolley stops, oscillation is again induced. When the desired command is no motion, there are two switch angle lines given by (14) and (15), as the crane can cancel the oscillation by going either forwards or backwards. The first switch angle occurs at a little after 13 seconds, and the crane moves forward slightly to cancel the oscillations. Once the crane is back at rest very little oscillation remains.

4.3. Controller response for disturbance rejection

Fig. 25 shows the response of the crane to a disturbance when the trolley is at rest. At a little after 1 second, the payload was disturbed. At about 3 seconds, the oscillation phase angle matched the switch angle condition, and the controller commanded the trolley to move forward. At a little past 4 seconds, the phase angle matched again, and the trolley was commanded to stop. When the trolley came to rest at about 5.5 seconds, the payload swing was less than one degree.

Fig. 26 shows the response to a very large disturbance. At about 1 second, the payload was pushed with a disturbance that is larger than a single on-off command could suppress. In this case, the first on-off control action starting at about 2.5 seconds suppressed the maximum possible oscillation, and

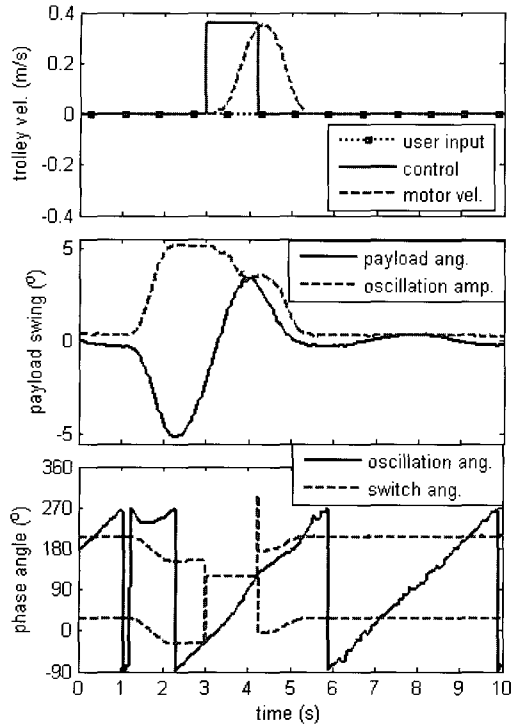

Fig. 25. Response to a disturbance while crane is at rest.

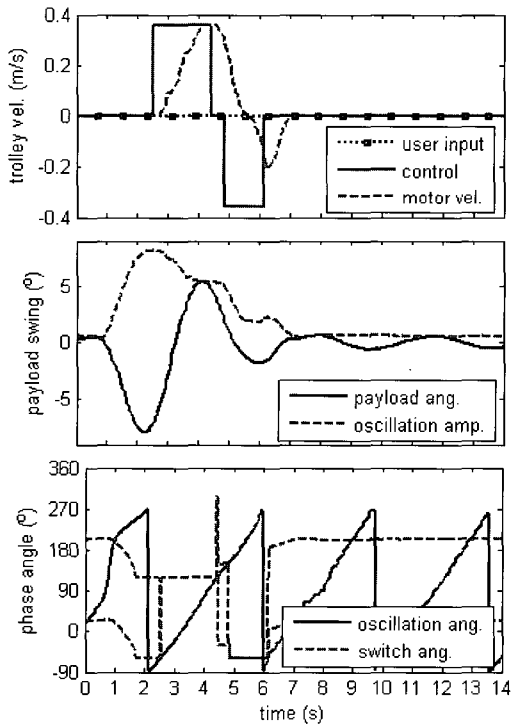

Fig. 26. Response to a large disturbance.

then the second control action canceled the remaining oscillation by moving the trolley in the opposite direction. This resulted in little oscillation after the crane had completed the second command at 6 seconds.

The controller can also eliminate disturbances while the crane is moving, as seen in Fig. 27. While the

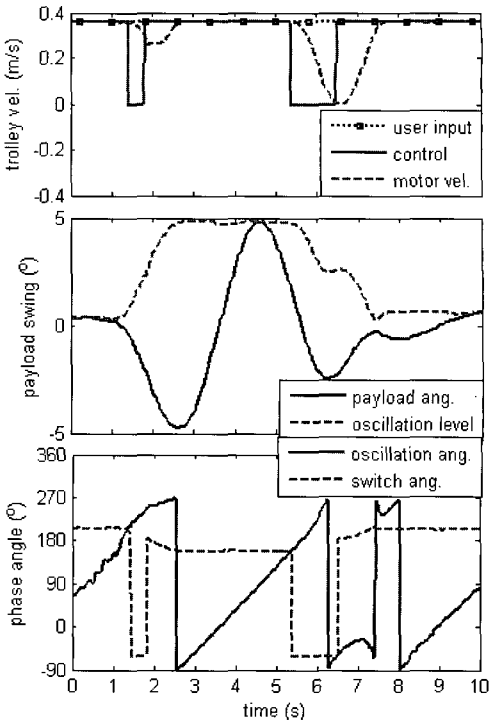

Fig. 27. Response to a disturbance when moving.

crane was moving forward with little oscillation, the payload was disturbed at about 1 second. The controller initially gives a stop command at about 1.5 seconds, which ceases shortly afterward (before the oscillation phase angle matched the switch angle, but based on the time safety factor from γ_{off}.) However, the payload was still being disturbed so the oscillations were not eliminated. The controller then waited until the appropriate phase angle, and then stopped the trolley again at about 6 seconds. At the appropriate time (7.5 seconds), the trolley accelerated resulting in little oscillation when the crane had returned to full speed.

5. CONCLUSION

A control strategy has been developed for motors using simple on-off commands to eliminate payload oscillations for bridge cranes. The control uses the computer vision measured swing angle of the payload, and its derivative, to decide when to turn the motors on and off. The method can reduce the oscillation when the crane is moving or at rest. The strategy was implemented on an industrial bridge crane. Numerous experiments demonstrated the control system effectiveness under a broad range of conditions. Future work could include verification of the control scheme on open loop AC induction motors and using the measured responses to adaptively modify the A_{on} and A_{off} vectors in the algorithm. Implementing the algorithm entirely within the camera is another possible extension of this work.

REFERENCES

[1] G. P. Starr, "Swing-free transport of suspended objects with a path-controlled robot manipulator," *Journal of Dynamic Systems, Measurement and Control*, vol. 107, no. 2, pp. 97-100, March 1985.

[2] J. Feddema, B. Petterson, and R. Robinett, "Operator control systems and methods for swing-free gantry-style cranes," U. S. Patent 5,785,191., 1998.

[3] N. Singer, W. Singhose, and E. Kriikku, "An input shaping controller enabling cranes to move without sway," presented at ANS 7th Topical Meeting on Robotics and Remote Systems, Augusta, GA, 1997.

[4] W. Singhose, L. Porter, M. Kenison, and E. Kriikku, "Effects of hoisting on the input shaping control of gantry cranes," *Control Engineering Practice*, vol. 8, no. 10, pp. 1159-1165, October 2000.

[5] W. E. Singhose, W. P. Seering, and N. C. Singer, "Input shaping for vibration reduction with specified insensitivity to modeling errors," *Proc. of the Japan-USA Sym. On Flexible Automation*, vol. 1, pp. 307-313, 1996.

[6] J. W. Auernig and H. Troger, "Time optimal control of overhead cranes with hoisting of the load," *Automatica*, vol. 23, no. 4, pp. 437-447, July 1987.

[7] J. J. Hamalainen, A. Marttinen, L. Baharova, and J. Virkkunen, "Optimal path planning for a trolley crane: Fast and smooth transfer of load," *IEE Proceedings Control Theory and Applications*, vol. 142, no. 1, pp 51-57, January 1995.

[8] A. J. Ridout, "Anti-swing control for the overhead crane using linear feedback," *Journal of Electrical and Electronics Engineering, Australia*, vol. 9, no. 1-2, pp. 17-26, 1989.

[9] K. A. F. Moustafa and A. M. Ebeid, "Nonlinear modeling and control of overhead crane load sway," *Journal of Dynamic Systems, Measurement, and Control*, vol. 110, no. 3, pp. 266-271, September 1988.

[10] H. T. Nguyen, "State-variable feedback controller for an overhead crane," *Journal of Electrical and Electronics Engineering, Australia*, vol. 14, no. 2, pp. 75-84, June 1994.

[11] H. Lee, "Modeling and control of a three-dimensional overhead crane," *Journal of Dynamic Systems, Measurement, and Control*, vol. 120, no. 4, pp. 471-476, December 1998.

[12] Y. S. Kim, K. S. Hong, and S. K. Sul, "Anti-sway control of container cranes: inclinometer, observer, and state feedback," *International Journal of Control, Automation, and Systems*, vol. 2, no. 4, pp. 435-449, December 2004.

[13] W. J. O'conner, "A gantry crane problem solved," *ASME Journal of Dynamics Systems, Measurement and Control*, vol. 125, no. 4, pp. 569-576, December 2003.

[14] Z. N. Masoud and A. H. Nayfe, "Sway reduction on container cranes using delayed feedback controller," *Nonlinear Dynamics*, vol. 34, no. 3-4, pp. 347-358, December 2003.

[15] K. Hekman, C. Stäheli, K. Sorenson, and W. Singhose, "Measuring crane payload swing angle through computer vision," *Proc. of the International Symposium on Flexible Automation*, Osaka, Japan, July 10-12, 2006.

[16] K. Sorensen, W. Singhose, and S. Dickerson, "A controller enabling precise positioning and sway reduction in bridge and gantry cranes," *Control Engineering Practice*, vol. 15, no. 7, pp. 825-837, July 2007.

[17] J. Y. Park and P. H. Chang, "Vibration control of a telescopic handler using time delay control and commandless input shaping technique," *Control Engineering Practice*, vol. 12, no. 6, pp. 769-780, June, 2004.

[18] J. P. Den Hartog, *Mechanical Vibrations*, 4th ed., McGraw-Hill, New York, 1956.

[19] H. G. Booker, *A Vector Approach to Oscillations*, Academic Press, New York, 1965.

[20] W. Singhose, W. Seering, and N. Singer, "Residual vibration reduction using vector diagrams to generate shaped inputs," *ASME Journal of Mechanical Design*, vol. 116, no. 2, pp. 654-659, June 1994.

Keith Hekman received the B.S. degree in Engineering from Calvin College, USA in 1992 and the M.S. and Ph.D. degrees from the Georgia Institute of Technology, USA in 1994 and 1997 respectively. He taught in the Mechanical Engineering Department at the American University in Cairo, Egypt from 1998 to 2005. Currently he is an Associate Professor in the Engineering Department at Calvin College. His research interests include command shaping and control of manufacturing processes.

William Singhose received the B.S. degree in Mechanical Engineering from the Massachusetts Institute of Technology, USA in 1990, the M.S. degree in Mechanical Engineering from Stanford University, USA in 1992 and the Ph.D. degree in Mechanical Engineering from the Massachusetts Institute of Technology, USA in 1997. In 1998 he joined the Georgia Institute of Technology as an Assistant Professor and is now an Associate Professor. His research interests include vibration, flexible dynamics, and command generation.